



JAAS

Morphological and chemical evidence for cyclic bone growth in a fossil hyaena

Journal:	<i>Journal of Analytical Atomic Spectrometry</i>
Manuscript ID	JA-ART-09-2018-000314
Article Type:	Paper
Date Submitted by the Author:	26-Sep-2018
Complete List of Authors:	<p>Anné, Jennifer; University of Manchester, School of Earth and Environmental Sciences; The Children's Museum of Indianapolis, Collections</p> <p>Wogelius, Roy; University of Manchester, School of Earth and Environmental Sciences</p> <p>Edwards, Nicholas; SLAC National Accelerator Laboratory; University of Manchester, School of Earth and Environmental Sciences</p> <p>van Veelen, Arjen; University of Southampton Faculty of Engineering and the Environment</p> <p>Buckley, Michael; University of Manchester, School of Earth and Environmental Sciences</p> <p>Sellers, William; University of Manchester, School of Earth and Environmental Sciences</p> <p>Bergmann, Uwe; SLAC National Accelerator Laboratory</p> <p>Sokaras, Dimosthenis; SLAC National Accelerator Laboratory, Stanford Synchrotron Radiation Lightsource</p> <p>Mori, Roberto; Stanford Synchrotron Radiation Lightsource, SLAC National Accelerator Laboratory,</p> <p>Harvey, Virginia; University of Manchester School of Earth and Environmental Sciences</p> <p>Egerton, Victoria; University of Manchester, School of Earth and Environmental Sciences; The Children's Museum of Indianapolis</p> <p>Manning, Phillip; University of Manchester, School of Earth and Environmental Sciences</p>



1 Morphological and chemical evidence for cyclic bone growth in a fossil hyaena

2
3 Jennifer Anné*^{1,2}, Roy A. Wogelius^{1,3}, Nicholas P. Edwards^{1,4}, Arjen van Veelen^{2,5}, Michael
4 Buckley¹, William I. Sellers¹, Uwe Bergmann⁴, Dimosthenis Sokaras⁴, Roberto Alonso-Mori⁴, Virginia L.
5 Harvey¹, Victoria M. Egerton^{1,2}, Phillip L. Manning¹

6
7 ¹University of Manchester, School of Earth and Environmental Sciences, Interdisciplinary Centre for
8 Ancient Life, Manchester M13 9PL, UK

9 ²The Children's Museum of Indianapolis, Indianapolis, IN, 46206, USA

10 ³University of Manchester, School of Earth and Environmental Sciences, Williamson Research Centre for
11 Molecular Environmental Science, Manchester M13 9PL, UK

12 ⁴SLAC National Accelerator Laboratory, Menlo Park, CA, 94025, USA

13 ⁵University of Southampton, Faculty of Engineering and the Environment, Southampton, SO17 1BJ, UK

14
15 * janne@childrensmuseum.org

17 ABSTRACT

18 Trace element inventories are known to correlate with specific histological structures in bone, reflecting
19 organismal physiology and life histories. By studying trace elements in fossilised bone, particularly in
20 individuals with cyclic bone growth (alternating fast/slow bone deposition), we can improve our
21 understanding of the physiology of extinct organisms. In this study we present the first direct comparison
22 between optical histology (bone tissue identification) and synchrotron-based chemical mapping,
23 quantification, and characterisation of trace elements (biochemistry) within cyclic growth tissues, in this
24 case within bones of a cave hyaena (*Crocota crocuta spelaea*). Results show distributions of zinc, an
25 element strongly associated with active ossification and bone growth, correlating with 1) fast-growing
26 tissue of zonal bone (cyclic growth) in an extinct hyaena and 2) secondary osteons (remodelling) in both
27 extant and extinct hyaena. Concentrations and coordination chemistry of zinc within the fossil sample are
28 comparable to those seen in extant bone suggesting that zinc is endogenous to the sample and that the
29 chemistry of bone growth has been preserved for 40 ka. These results demonstrate that the study of trace
30 elements as part of the histochemistry have wide utility for reconstructing growth, diet and other lifestyle
31 factors in archaeological and fossil bone.

34 INTRODUCTION

35 The physiology and life history of vertebrates are reflected in the microstructure of their skeletons
36 (histology). As most vertebrate remains are preserved solely as bones, these tissues can provide key
37 information on the physiology of extinct organisms such as metabolism and biological cycles. It is
38 through such studies that we are able to identify key changes in vertebrate physiology through time,
39 highlighting the adaptability of vertebrates to new and/or changing environments.

40
41 One of the physiological processes recorded in bone is the growth rate throughout an individual's life,
42 which can be characterised by cyclic growth. These are fluctuations in bone depositional rates recognised
43 in histological sections as alternating bands, known as zonal tissues, which are indicative of slow and fast
44 growth¹⁻⁷. It has previously been presumed that zonal bone is a characteristic of poikilothermic (slow
45 metabolism) physiology due to the association of homeotherms (fast metabolism) with uninterrupted high
46 rates of growth until maturity²⁻⁴. This paradigm has recently been challenged with the identification of
47 zonal bone in a wide range of fossil and extant mammalian and avian groups^{1-3,5-7}. However, it is still
48 unclear how widespread zonal bone is within vertebrates, and thus what controls are placed on the
49 plasticity of bone growth. Zonal bone formation has been attributed to changes in food/water sources,
50 changes in temperature/thermoregulation, migration, sexual maturity and reproduction^{2,4,6}. As stress
51 affects the biochemical signalling that controls the rate of bone deposition, it is likely that mediating
52 factors behind such signalling, such as compositional differences, may also be preserved within zonal
53 tissues.

54
55 In addition to changes in bone microstructure, changes in bone physiology can also be characterised
56 through trace element inventories. Previous studies have shown that the key trace elements for bone
57 physiology (most notably Cu, Zn and Sr) can be mapped within discrete histological features, which
58 correlate to specific physiological processes such as active ossification and remodelling⁸⁻¹⁵. The distinct
59 association with trace metals is a function of low concentrations (ppm) of organometallic compounds
60 necessary for bone development, health and function, and the catalysis of enzymatic processes. Thus trace
61 element inventories in bone can indicate the activity of physiological processes such as changes in bone
62 growth. As zonal bone represents alternating fast (zones) and slow (annuli) depositional tissues, the trace
63 element inventories associated with bone growth should reflect these changes in depositional rates.
64 Therefore, by comparing differences in chemical inventories between the two tissue types, we can gain a
65 better understanding of the physiological processes that control the switch between the two depositional
66 rates.

67

1
2
3 68 Until recently, investigations into such chemical/histological correlations have not been attempted as
4 69 commonly available techniques are unable to resolve the discrete variations (ppm levels) in chemistry at
5 70 the necessary resolution (micron) and scale (decimetre). However, recent work using synchrotron-based
6 71 X-Ray Fluorescence (XRF) has demonstrated the ability to resolve the chemical variations associated
7 72 within fine scale histological features in extant and fossil bone⁸⁻¹³. Here we present the first histological
8 73 and trace element analyses of bones from extinct cave hyaena (*Crocota crocuta spelaea*) and extant
9 74 spotted hyaena (*Crocota crocuta*) to determine 1) whether cyclic growth can be correlated with
10 75 differential distributions of trace elements crucial for bone growth and 2) if these elements can be
11 76 preserved in fossilised tissues. Hyaenas were chosen based on the identification of zonal bone in other
12 77 Pleistocene mammals and in extant arctic carnivores, both of which experience extremely high seasonal
13 78 stress^{1-2,5}. Cave hyaena are also very closely related to extant hyaena species (subspecies of spotted
14 79 hyaena), thus limiting the amount of change in physiology due to taxonomic separation distance.
15
16
17
18
19
20
21
22
23

24 81 METHODS

25 82 *Specimens*

26 83 Specimens consisted of four extant spotted hyaena (*C. crocuta*; ribs; fig. S1) consisting of both male
27 84 (AMNH 87769, 83593) and female (AMNH 114226, 114227) specimens, and three extinct cave hyaena
28 85 (*C. c. spelaea*; radius LL.20879, metacarpal LL.2200 and limb bone fragment P.3062; fig. S2). All extant
29 86 specimens are from the American Museum of Natural History, New York, NY. The fossil specimen
30 87 (P.3062) is from the Manchester Museum, Manchester, UK. Unfortunately, the same set of skeletal
31 88 elements could not be sampled for both extant and fossil specimens due to the fragmentary nature of the
32 89 fossil samples and the restrictions on destructive sampling of limb bones from extant material. Samples of
33 90 bone from extant hyaena represent individuals that had been wild caught as captive animals are less likely
34 91 to develop zonal tissue due to conditions provided in captivity (ex. zoo). Fossil material was obtained
35 92 from the Pin Hole (radius LL.20879 and metacarpal LL.2200; 37.8 ka) and Church Hole Caves (indent.
36 93 fragment P.3062; 26.84 to 24 ka), Creswell Crags, UK (fig.S3)¹⁶. Due to the fragmented nature of the
37 94 limb bone, faunal identification was confirmed using collagen fingerprinting (fig. S4)¹⁷.
38
39
40
41
42
43
44
45
46

47 96 *Optical Histology*

48 97 Thin sections were cut to a final thickness of ~25-50 µm. Sections were viewed using a Nikon ECLIPSE
49 98 E600 POL microscope and ACT-1 software and a Leica DM2700P microscope and Leica Application
50 99 Suite software under plain polarized and cross polarized light at 2x, 4x, and 10x magnifications. The billet
51 100 or 'thick section' left from the thin section was used for chemical analyses, with no further sample
52 101 preparation performed.
53
54
55
56
57
58
59
60

102

Synchrotron Analyses

Synchrotron Rapid Scanning X-Ray Fluorescence (SRS-XRF) was conducted at beamline 6-2 at the Stanford Synchrotron Radiation Lightsource (SSRL; CA, USA). Detailed descriptions of SRS-XRF mapping applied to fossils are provided in recent publications^{9,18-23} and are summarised here. Maps were collected with an incident beam energy of either 13.5 keV (high-Z; Ca and higher) or 3.15 keV (low-Z; Ca and lower). Specimens were mounted on an x-y-z stage and rastered relative to the fixed incident beam, with a 50 µm (fossil specimen) or 25 µm (extant specimens) beam diameter ('large-scale'). Areas of interest in the fossil hyaena identified by SRS-XRF mapping were then mapped at higher spatial resolution at the Diamond Light Source (DLS; Oxfordshire, UK), beamline I-18, using the experimental setup of^{8-9,19}. Maps were made using 5.5 µm beam diameter produced via Kirkpatrick-Baez focusing mirrors, with incident beam energy of 17 keV (chosen to allow excitation of the Sr K α emission). X-ray flux was 10¹⁰ - 10¹¹ photons s⁻¹ ('microfocus').

Single location energy dispersive spectra (EDS) were taken at both synchrotrons to quantify elements in discrete features (identified on elemental maps) by collecting a full EDS for 50 sec (SSRL) or 30 sec (DLS). Multiple spectra were taken per area of interest to account for heterogeneity within the sample. Spectra were fitted using PyMCA software (ex. fig. S5)²⁴. A Durango apatite mineral standard of known element concentrations was used for calibration.

Zinc Extended X-ray Absorption Fine Structure spectroscopy (EXAFS) was performed at DLS beamline I-18 to k space =12. The Zn K-edge was calibrated using a Zn-foil. Background subtraction, data normalization and fitting were performed using (d) Athena and (d) Artemis²⁵. Spectra were compared to extant mammal bone and Zn-Hydroxyapatite (HAP) references²⁶.

RESULTS**Optical Histology**

Optical histology of the extant *C. crocuta* ribs shows a combination of densely packed secondary osteons ('2°'; fig. 1) and areas of woven tissue running through the specimen into the cancellous struts ('W'; fig. 1). No apparent differences between male (AMNH 187769 and 83593) and female (AMNH 114226 and 114227) specimens were observed.

Optical histology of the extinct *C. c. spelaea* radius and metacarpal (LL.20879 and LL.2200) revealed similar histological patterns as the extant material, with a mixture of woven bone ('W'; fig. 2A, F) and

1
2
3 136 secondary osteons ('2°'; fig. 2A-B). Additional histological features include primary ('1°'; fig. 2D) and
4 137 drifting ('D'; fig. 2E) osteons (osteon running both longitudinally and transversely through cortex). The
5 138 radius also shows fabric that is oriented obliquely to the more remodelled internal bone tissue situated
6 139 around the outer cortex (fig.2 C). The fossil limb bone fragment (P.3062) shows zonal bone growth, seen
7 140 as alternating bands of fast-growth (zones) and slow-growth (annuli) fibrolamellar tissues (brackets; fig.
8 141 2G-H). Zones are identified by elongated osteons with large canal openings aligned in a 'ring' following
9 142 the circumference of the bone section ('Z'; fig. 2H). Annuli are identified by tightly packed lamellar bone
10 143 forming another 'ring' ('A'; fig. 2H). Thus, zones are identified as areas of bone tissue that are
11 144 significantly more vascularised than annuli. A series of secondary osteons is seen in two isolated
12 145 locations, with the osteons overprinting the original cortex through the entire cortical thickness ('2°'; fig.
13 146 2I).

147 148 ***SR-XRF***

149 XRF large-scale mapping (decimetre scale) shows Zn to be concentrated within secondary osteons (arrow
150 and inset; fig. 3). Differences in the elemental inventories between male and female are seen in Ca, Mn
151 and As, with higher concentrations seen in female specimens (fig. 3; Table 1; Table S1). No other
152 elements could be correlated with specific histological features or tissue types.

153
154 Large-scale (centimetre) and microfocus elemental maps of the extinct *C. c. spelaea* limb bone fragment
155 (P.3062) are presented in figure 4. Elemental maps of Zn revealed a pattern of relative high and low Zn
156 banding (arrow; fig. 4C). These bands were shown to correlate with the cyclic bands of zones and annuli,
157 with higher concentrations in zones ('Z'; fig. 4D). As in extant hyaena, Zn was also found to be
158 associated with secondary osteons (circle; fig. 4D). Arsenic is elevated within the medullary cavity and a
159 section of the cortical bone not associated with the zones (fig. 4E), and is present within the primary bone
160 tissue, but not within secondary osteons (fig. 4F; circle). Fe is elevated within the medullary cavity (fig.
161 4G) and areas of mineral infill (fig. 4H; arrows). Sr is slightly elevated within the cement rings of the
162 osteon (fig. 4I; circle).

163
164 Trace element concentrations from the fossil limb bone fragment (P.3062) are within the range known for
165 extant material^{8-10, 27}, with slight depletion in Ca and enrichment in Fe and Sr (Table 1). Elevated areas of
166 Zn are approximately double the concentration of "low" Zn areas. Concentrations from non-elevated
167 areas are comparable to cortical bone concentrations from extant material scanned in this study (Table 1).

1
2
3 169 ***Spectroscopy***

4
5 170 X-ray absorption spectroscopy was performed to determine the coordination chemistry Zn within the
6
7 171 bones in order to investigate whether the Zn could be derived from the original biochemistry of the
8
9 172 organisms or if it had been replaced through taphonomic processes. Zn EXAFS of P.3062 revealed a
10
11 173 tetrahedral coordination with four-O atoms at a distance of 1.95 Å (Table 2). This coordination and
12
13 174 spacing is comparable to modern tissues (fig. 5; Table 2), and Zn-HAP with concentrations of Zn
14
15 175 comparable to modern bone (200-400 ppm), suggesting Zn was precipitated into the tissue during growth
16
17 176 and is not surface contamination.

17 177
18 178 **DISCUSSION**

19 179 The combination of optical and chemical histological analyses revealed Zn to be correlated within the fast
20
21 180 growth tissues (zones) of zonal bone within an extinct cave hyaena (*C. c. spelaea*) limb fragment (P.3062;
22
23 181 fig. 4C-D) and within areas of active remodelling in extant hyaena (*C. crocuta*; fig. 2) and cave hyaena
24
25 182 (fig. 4C-D). This observation fits with previous studies showing that enhanced Zn concentrations can be
26
27 183 found within areas of active ossification and bone growth^{8-11, 13-15}, and that Zn is stable within the apatite
28
29 184 structure of bone for extended periods of geologic time^{8-9, 12, 27}.

30 185
31 186 This study reports the first case of zonal tissue within the Hyaenidae, both extant and fossil. The series of
32
33 187 alternating high and low vascularity is interpreted as zonal tissue based on the regular deposition over a
34
35 188 large area of the external cortex, which suggests deposition over time. It is not possible to state that each
36
37 189 pair of zones/annuli correlates to one year of growth as there are numerous potential physiological and
38
39 190 environmental factors that could also result in this alternating deposition (as discussed in the
40
41 191 introduction). Intrasketal variation could be one of the reasons for the lack of zonal tissue seen in the
42
43 192 other two fossil hyaena (radius and metatarsal). It is interesting to note that the fossil hyaena displaying
44
45 193 cyclic growth is from a stadial (colder phase; ~25 ka) of the last ice age, whereas the specimens without
46
47 194 annual zones are from an interstadial (warmer phase; ~38 ka)²⁸. Future work is needed to test the
48
49 195 hypothesis of whether extreme seasonal differences may have caused the differences observed between
50
51 196 individuals.

52
53 197
54 198 Concentrations of Zn follow the pattern of zones and annuli, with higher concentrations correlating to
55
56 199 zones (high rates of bone deposition). The correlation between high Zn and increased bone deposition fits
57
58 200 within previous observations that Zn is important in areas of active growth such as around growth plates
59
60 201 and within osteons^{8,10,13-15}. Zn levels within the zones of the fossil limb fragment (P.3062) are higher than
202 the average concentrations measured in extant hyaena in this study, but are within the range seen in other

1
2
3 203 terrestrial carnivores and humans^{10,27}. The elevated regions within the zones are thin, and therefore the
4 204 average Zn concentration in the fossil bone will be closer to reported bulk Zn concentrations in unzoned
5 205 bone. EXAFS spectroscopy shows that the Zn is positively associated with fossil bone tissue, most
6 206 notably the fast-growth zonal tissues, strengthening the hypothesis that Zn is endogenous to the specimen
7 207 (fig. 5C-D).

8 208
9
10
11
12 209 Elemental mapping also revealed interesting distributions of As, Fe and Sr within the fossil limb bone
13 210 fragment (P.3062). Arsenic is associated with zonal tissue, though it is completely absent within osteons
14 211 (fig. 4E-F). In extant specimens, it is difficult to discern the origins of As given concentrations of As in
15 212 the extant bone samples are variable probably due to its occasional use as a preserving agent in museum
16 213 collections. Therefore we should not attempt to compare concentrations of As between the extant and
17 214 fossil specimens. Concentrations of Fe suggest some diagenetic input as Fe levels are slightly elevated
18 215 compared to extant bone (Fe 10-50 ppm; Goodwin et al., 2007; Table 1), but not as heavily elevated as
19 216 those seen in archaeological/fossil specimens (Fe 500-60,000 ppm)²⁹⁻³⁰. Sr distributions show lower
20 217 concentrations of Sr within secondary osteons compared to the surrounding tissue, with the exception of
21 218 the cement lines that form as the osteon is filled in by separate layers of lamellar bone (fig. 4I).
22 219 Concentrations of Sr are between expected levels for extant terrestrial carnivores²⁷ and recent
23 220 archaeological samples (less than 1,000 years old)^{11,29} suggesting little to no diagenetic input.

221 222 CONCLUSION

223 Correlation between histological features and chemical inventories strengthen the link between
224 morphology and physiological processes, generating a *de novo* approach to the study of extinct
225 organismal physiology. In this study, cyclic growth was correlated with differential distribution of Zn
226 between fast (zones) and slow (annuli) growing bone tissue in the limb fragment of an extinct cave
227 hyaena, *C. c. spelaea* (P.3062). The ability to resolve the subtle difference in biological chemistry
228 between bone tissue types was only possible using the multi-scale mapping capabilities of synchrotron
229 analyses. These results highlight the implications of using trace-element markers as a means for
230 improving the analysis of archaeological and fossil bone.

231 232 ACKNOWLEDGEMENTS

233 We thank the Stanford Synchrotron Radiation Lightsource (3959) and Diamond Light Source (SP9488),
234 the Manchester Museum (U.K), Academy of Natural Sciences of Drexel University (USA), American
235 Museum of Natural History (USA), all support staff at SSRL and Professor Andrew Chamberlain for his
236 invaluable advice

1
2
3 237

4
5 238 FUNDING

6 239 All authors acknowledge financial support from NERC (NE/J023426/1), the Royal Society (UF120473),
7 240 the Jurassic Foundation (awarded JA), and the University of Manchester Dean's Award Fund (awarded
8 241 JA). PLM thanks the Science and Technology Facilities Council for their support (ST/M001814/1).

9
10 242

11
12 243 AUTHOR CONTRIBUTIONS

13
14 244 All authors contributed in the synchrotron analysis and commented on the manuscript. JA, RAW and
15 245 PLM designed the experiment. JA performed the optical histological analysis, processed the synchrotron
16 246 data, wrote the manuscript and composed the figures. AvV processed and fit the EXAFS data, and
17 247 composed figure 5 and table 2. MB conducted the proteomics analyses (Supp. Material).

248 REFERENCES

- 249 1. Köhler, M., Marin-Moratalla, N., Jordana, X. and Aanes, R. Seasonal bone growth and
250 physiology in endotherms shed light on dinosaur physiology. *Nature*. 2012; 487: 358-361.
251 doi:10.1038/nature11264.
- 252 2. Chinsamy-Turan, A. Forerunners of Mammals: Radiation Histology Biology (Life of the Past).
253 Bloomington: Indiana University Press. 2011.
- 254 3. Köhler, M. and Moyà-Solà, S. Physiological and life history strategies of a fossil large mammal
255 in a resource-limited environment. *P Natl. Acad. Sci. USA*. 2009; 106(48): 20354–58.
- 256 4. Castanet, J. Time recording in bone microstructures of endothermic animals; functional
257 relationships. *C. R. Palevol*. 2006; 5: 629-636.
- 258 5. Chinsamy-Turan, A. The Microstructure of Dinosaur Bone: Deciphering Biology with Fine-scale
259 Techniques. Baltimore: The Johns Hopkins University Press. 2005.
- 260 6. Chinsamy, A. and Dodson, P. Inside a dinosaur bone. *Am. Sci*. 1995; 83: 174-180.
- 261 7. Kolb, C., Scheyer, T.M., Veitschegger, K., Forasiepi, A.M., Amson, E., Van der Geer, A.A.E., et
262 al. Mammalian bone palaeohistology: a survey and new data with emphasis on island forms.
263 *PeerJ*. 2015; 3: e1358.
- 264 8. Anné, J, Wogelius, R.A., Edwards, N.P., van Veelen, A., Ignatyev, K. and Manning, P.L.
265 Chemistry of bone remodelling preserved in extant and fossil Sirenia. *Metallomics*. 2016; 8(5):
266 508-513. doi: 10.1039/C5MT00311C.
- 267 9. Anné, J., Edwards, N.P., Wogelius, R.A., Tumarkin-Deratzian, A.R., Seller, W.I., van Veelen, A.,
268 et al. Synchrotron imaging reveals bone healing and remodelling strategies in extinct and extant
269 vertebrates. *J. R. Soc. Interface*. 2014; 11(96): 20140277–20140277.
- 270 10. Pemmer, B., Roschger, A., Wastl, A., Hofstaetter, J.G., Wobraschek, P., Simon, R., et al. Spatial
271 distribution of the trace elements zinc, strontium, and lead in human bone tissue. *Bone*; 2013; 57:
272 184-193.
- 273 11. Swanston, T., Varney, T., Coulthard, I., Feng, R., Bewer, B., Murphy, R., et al. Element
274 localization in archaeological bone using synchrotron radiation x-ray fluorescence: Identification
275 of biogenic uptake. *J. Archaeol. Sci*. 2012; 39(7): 2409–13. doi:10.1016/j.jas.2012.01.041
- 276 12. Kuczumow, A., Cukrowska, E., Stachniuk, A., Gawęda, R., Mroczka, R. Paszkowicz, W., et al.
277 Investigation of chemical changes in bone material from South African fossil hominid deposits. *J.*
278 *Archaeol. Sci*. 2010; 37: 107–115
- 279 13. Molokwu, C.O. and Li, Y.V. Zinc homeostasis and bone mineral density. *Ohio Res. Clin. Rev*.
280 2006; 15: 7–15.

- 1
2
3 281 14. Hammond, G.L., Avvakumov, G.V. and Muller, Y.A. Structure/function analyses of human sex
4 282 hormone-binding globulin: Effects of zinc on steroid-binding specificity. *J. Steroid Biochem.*
5 283 2003; 85(2-5): 195–200. doi:10.1016/S0960-0760(03)00195-X.
6
7 284 15. Gomez, S., Rizzo, R., Pozzi-Mucelli, M., Bonucci, E. and Vittur, F. Zinc mapping in bone tissues
8 285 by histochemistry and synchrotron radiation-induced x-ray emission: Correlation with the
9 286 distribution of alkaline phosphates. *Bone*. 1999; 25(1): 33-38.
10
11 287 16. Hedges, R.E.M, Pettitt, P.B., Ramsey, C.B. and van Klinken, G.J. Radiocarbon dates from the
12 288 Oxford AMS system: *Archaeometry* datelist 22. *Archaeometry*. 1996; 38(2): 391-415.
13
14 289 17. van der Sluis, L.G., Hollund, H.I., Buckley, M., De Louwd, P.G.B., Rijdsdijke, K.F., Kars, H.
15 290 Combining histology, stable isotope analysis and ZooMS collagen fingerprinting to investigate
16 291 the taphonomic history and dietary behaviour of extinct giant tortoises from the Mare aux Songes
17 292 deposit on Mauritius. *Palaeogeogr. Palaeoclimatol. Palaeoecol.* 2014; 416: 80-91.
18
19 293 18. Egerton V., Wogelius, R.A., Norell, M.A., Edwards, N.P., Sellers, W.I., Bergmann, U., et al. The
20 294 mapping and differentiation of biological and environmental elemental signatures in the fossil
21 295 remains of a 50 million year old bird. *J. Anal. At. Spectrom.* 2015; 30: 627-634.
22 296 doi: 10.1039/C4JA00395K
23
24 297 19. Edwards, N.P., Manning, P.L., Bergmann, U., Larson, P.L., van Dongen, B.E, Sellers, W.I, et al.
25 298 Leaf metallome preserved over 50 million years. *Metallomics*. 2014; 6(4): 774-782.
26
27 299 20. Manning, P.L., Edwards, N.P., Wogelius, R.A., Bergmann, U., Barden, H.E., Larson, P., et al.
28 300 Synchrotron-based chemical imaging reveals plumage patterns in a 150 million year old early
29 301 bird. *J. Anal. At. Spectrom.* 2013; 28(7): 1024-1030. doi:10.1039/c3ja50077b.
30
31 302 21. Edwards, N.P., Wogelius, R.A., Bergmann, U., Larson, P., Sellers, W.I. and Manning, P.L.
32 303 Mapping prehistoric ghosts in the synchrotron. *Appl. Phys. A Mater. Sci. Process.* 2013; 111(1):
33 304 147–155. doi:10.1007/s00339-012-7484-3.
34
35 305 22. Wogelius, R.A., Manning, P.L., Barden, H.E., Edwards, N.P., Webb, S.M., Sellers, W.I., et al.
36 306 Trace metals as biomarkers for eumelanin pigment in the fossil record. *Science*. 2011; 333(6049):
37 307 1622–1626. doi:10.1126/science.1205748.
38
39 308 23. Bergmann, U., Morton, R.W., Manning, P.L., Sellers, W.I., Farrar, S., Huntley, K.G., et al.
40 309 *Archaeopteryx feathers* and bone chemistry fully revealed via synchrotron imaging. *Proc Natl*
41 310 *Acad Sci.* 2010; 107(20): 9060-9065.
42
43 311 24. Solé, V.A., Papillon, E., Cotte, M., Walter, Ph. and Susini, J. A multiplatform code for the
44 312 analysis of energy-dispersive X-ray fluorescence spectra. *Spectrochim. Acta B.* 2007; 62(1): 63–
45 313 68. doi:10.1016/j.sab.2006.12.002.
46
47
48
49
50
51
52
53
54
55
56
57
58
59
60

- 1
2
3 314 25. Ravel, B. and Newville, M. Athena, Artemis, Hephaestus: Data Analysis for X-ray Absorption
4 315 Spectroscopy using IFEFFIT. *J. Synchrotron Radiat.* 2005; 12: 537-541. doi:
5 316 10.1107/S0909049505012719.
6
7
8 317 26. Tang, Y., Chappell, H.F., Dove, M.T., Reeder, R.J. and Lee, Y.J. Zinc incorporation into
9 318 hydroxylapatite. *Biomaterials.* 2009; 30(15): 2864–2872.
10
11 319 27. Sealy, J.C. and Sillen, A. Sr and Sr/Ca in marine and terrestrial foodwebs in the southwestern
12 320 cape, South Africa. *J. Archaeol. Sci.* 1988; 15: 425-438.
13
14 321 28. Rasmussen, S.O., Bigler, M., Blockley, S.P., Blunier, T., Buchardt, S.L., Clausen, H.B. et al. A
15 322 stratigraphic framework for abrupt climatic changes during the Last Glacial period based on three
16 323 synchronized Greenland ice-core records: refining and extending the INTIMATE even
17 324 stratigraphy. *Quat. Sci. Rev.* 2014; 106: 14-28.
18
19 325 29. Carvalho M.L., Marques, A.F., Lima M.T. and Reus, U. Trace elements distribution and post-
20 326 mortem intake in human bones from middle age by total reflection X-Ray fluorescence.
21 327 *Spectrochim. Acta B.* 2004; 59(8): 1251-1257.
22
23 328 30. Goodwin, M.B., Grant, P.G., Bench, G. and Holroyd, P.A. Elemental composition and diagenetic
24 329 alteration of dinosaur bone: Distinguishing micron-scale spatial and composition heterogeneity
25 330 using PIXE. *Palaeogeogr. Palaeoclimatol. Palaeoecol.* 2007; 253: 358-476.
26
27
28
29
30
31
32
33
34
35
36
37
38
39
40
41
42
43
44
45
46
47
48
49
50
51
52
53
54
55
56
57
58
59
60

331 TABLE and TABLE CAPTIONS

	Mineral Standard	<i>C. crocuta</i> (avg)		<i>C. c. spelaea</i> Fragment	
		Male	Female	Annuli	Zone
Ca	38.38% (2.27%)	32.19% (2.06%)	36.42% (2.26%)	23.47% (0.81%)	25.13% (0.78%)
Mn	-	2 (0.4)	133 (26)	56 (8)	145 (16)
Fe	902 (30)	37 (4)	51 (8)	136 (17)	175 (20)
Cu	-	5 (1)	3 (1)	1 (0.2)	3 (0.5)
Zn	77 (3)	130 (9)	134 (10)	165 (16)	384 (31)
As	2185 (68)	11 (1)	389 (21)	9 (1)	3 (0.4)
Sr	1885 (47)	-	-	421 (23)	405 (20)

332 **Table 1:** Synchrotron XRF quantification of trace elements taken at SSRL (extant *C. crocuta*) and DLS
 333 (extinct *C. c. spelaea*; P.3062) given in ppm or weight percent (%). Extant *C. crocuta* measurements
 334 represent an average over the cortical bone as no zonal tissues were present. Fit errors are given in
 335 parentheses and represent \pm two standard deviations.

336

Specimen	Path	CN	R(Å)	$\sigma^2(\text{Å}^2)$	$\Delta E_0(\text{eV})$	S0 ²	χ^2	R
Extant	Zn-O	4.4	1.95(07)	0.007(1)	1.95 ± 0.77	0.99(3)	92	0.01
Fossil	Zn-O	4.2	1.95(05)	0.007(0.09)	2.14 ± 0.56	1.00(2)	17.26	0.007
Zn HAP (412 ppm) ²⁶	Zn-O	4.4	1.96	0.005	-0.53	-	-	0.073

337 **Table 2:** Fit statistics for Zn EXAFS in extant bone and P.3062 using (d) Artemis (5) and HAP with 412
 338 ppm Zn taken from ²⁶. Errors are given as (\pm) the last significant figure unless specified. Error for CN is
 339 25%. CN—coordination number; R(Å)—atomic distance (Å); $\sigma^2(\text{Å}^2)$ —Debye-Waller factor; $\Delta E_0(\text{eV})$ —
 340 shift in energy from calculated Fermi level; S0²—amplitude factor; R—goodness of fit.

341

342 FIGURE CAPTIONS

343 **Figure 1: Optical histology of extant hyeana.** Optical histology under cross-polarized light of *C.*
 344 *crocuta* ribs in adult male (AMNH 187769, 83593) and female (AMNH 114226, 114227) specimens. All
 345 specimens can be divided into two tissue types: highly remodelled with secondary osteons ('2°') or woven
 346 tissues ('W'). Scale bar is 200 μm .

1
2
3 347
4
5 348 **Figure 2: Optical histology for cave hyeana.** Optical histology of the extinct cave hyaena, *C. c. spelaea*,
6 349 radius (LL.20879; A-C), metacarpal (LL.2200; D-F) and limb fragment (P.3062; G-I) under cross
7 350 polarized light. The radius consists of areas of secondary osteons ('2°'; A-B) and woven bone ('W'; A).
8 351 In some regions, the periosteal surface has a fabric that is oriented obliquely to the more remodelled
9 352 internal bone tissue (C). The metatarsus consists of dense primary osteons ('1°'; D) and drifting osteons
10 353 ('D': E) interspersed with woven bone ('W'; F). Zonal bone is recognized in the limb fragment (G-H)
11 354 with zones characterised by high porosity, with elongated osteons ('Z'; H) and annuali characterised by
12 355 densely compact lamellar bone between annuali ('A'; H). A mass of secondary osteons is present,
13 356 crossing perpendicular to the zones ('2°'; I).

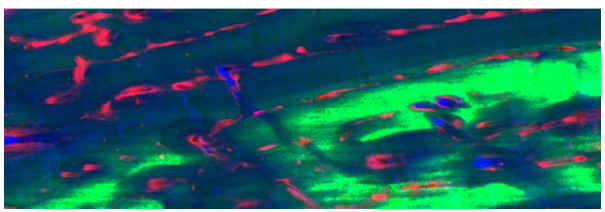
14 357
15
16 358 **Figure 3: Elemental maps of extant hyaena.** Optical large-scale (centimetre) elemental maps of Zn and
17 359 As in *C. crocuta* ribs (extant: male AMNH 87769, 83593; female AMNH 114226, 114227; fossil:
18 360 P.3062). Bright areas represent relatively higher concentrations (photon counts). The counts in each
19 361 elemental map are converted to 8 bit tiff images (scaled from 0 to 255) and thus is independently scaled
20 362 and does not represent relative intensities compared to another elemental map. In Zn, higher
21 363 concentrations (white) are associated with remodelling in secondary osteons (arrow and inset).
22 364 Concentrations of As are elevated in the two female samples (AMNH 114226, 114227), but is uniformly
23 365 distributed throughout the bone cross section. Scale bar is 1 cm.

24 366
25
26 367 **Figure 4: Elemental maps of cave hyena specimen P.3062.** Optical large-scale (centimetre) and
27 368 histological images (A,B) of *C. c. spelaea* limb fragment (P.3062) compared to large and fine scale
28 369 elemental maps of Zn (C,D), As (E,F), Fe (G,H) and Sr (I). Boxes on the large-scale images represent
29 370 areas of interest highlighted in microfocus. Large-scale elemental maps of Sr are unavailable due to not
30 371 being able to achieve the excitation energy for Sr on beamline 6-2 at SSRL. Bright areas represent
31 372 relatively higher concentrations (photon counts). The counts in each elemental map are converted to 8 bit
32 373 tiff images (scaled from 0 to 255) and thus is independently scaled and does not represent relative
33 374 intensities compared to another elemental map. Large-scale elemental mapping shows regular banding of
34 375 high/low Zn (arrow; C). Microfocus mapping shows these bands are correlated to the differences in zonal
35 376 tissue, with higher Zn concentration correlated to zones ('Z'; D). Higher concentrations of Zn are also
36 377 seen in association with secondary osteons (circle; D). In the large image, As is seen to be concentrated
37 378 within the medullary cavity and a section of the cortical bone not associated with the Zn banding (E).
38 379 However, in microfocus imaging bands of As do correlate to the differences in zonal tissue, with higher
39 380 concentration correlated to zones ('Z'; F). Arsenic is also anti-correlated with secondary osteons (circle;

1
2
3 381 F). Fe is mainly concentrated within the medullary cavity (G) and the mineral infill within osteon canals
4 382 (arrow; H). Sr is slightly depleted within secondary osteons, with the exception of elevated 'rings' seen in
5 383 the osteon highlighted (circle; I). Scale bar is 1 cm for large-scale images and 1 mm for microfocus.
6
7

8 384
9 385 **Figure 5: Zinc EXAFS.** Comparison of the Zn EXAFS spectra from the fossil and extant bone in k (A)
10 386 and R-space (B) show Zn coordination is identical in the fossil and extant bone tissues.
11
12
13
14
15
16
17
18
19
20
21
22
23
24
25
26
27
28
29
30
31
32
33
34
35
36
37
38
39
40
41
42
43
44
45
46
47
48
49
50
51
52
53
54
55
56
57
58
59
60

1
2
3
4
5
6
7
8
9
10
11
12
13
14
15
16
17
18
19
20
21
22
23
24
25
26
27
28
29
30
31
32
33
34
35
36
37
38
39
40
41
42
43
44
45
46
47
48
49
50
51
52
53
54
55
56
57
58
59
60



Our study is the first to correlate differential distributions of trace elements within the different tissue types of zonal bone.

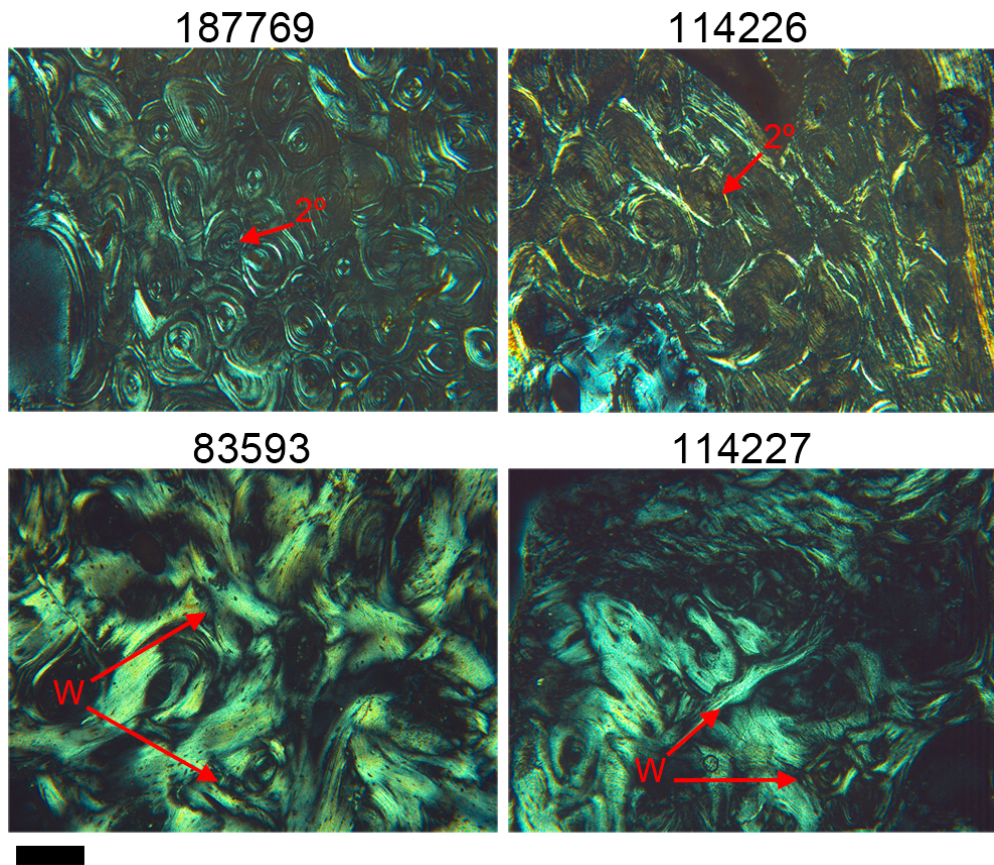
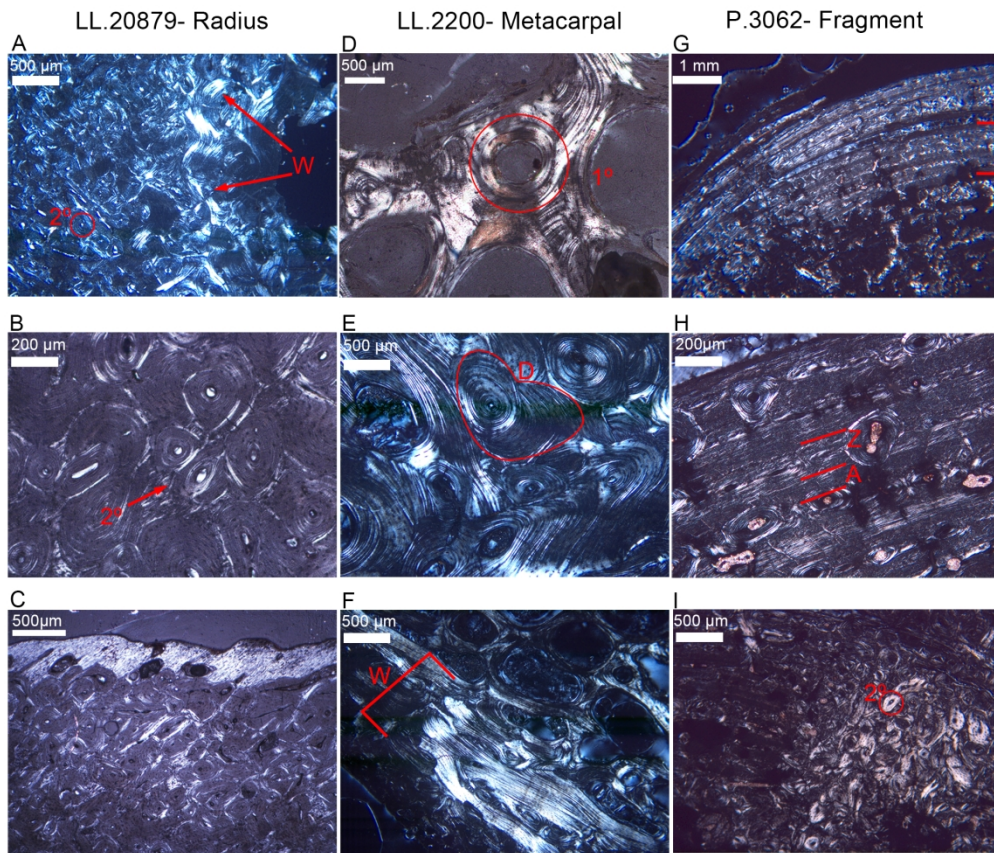


Figure 1: Extant hyena histology

83x72mm (300 x 300 DPI)



34 Figure 2: Fossil hyena histology

35 176x149mm (300 x 300 DPI)

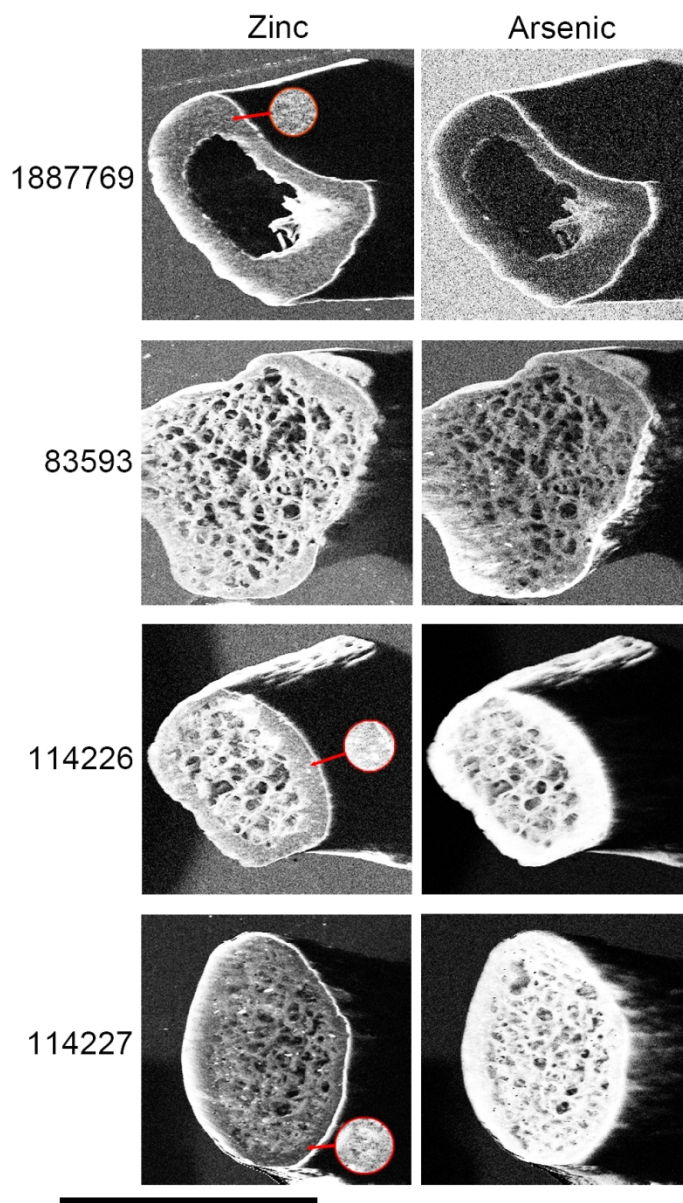


Figure 3: Extant hyena XRF maps

84x146mm (300 x 300 DPI)

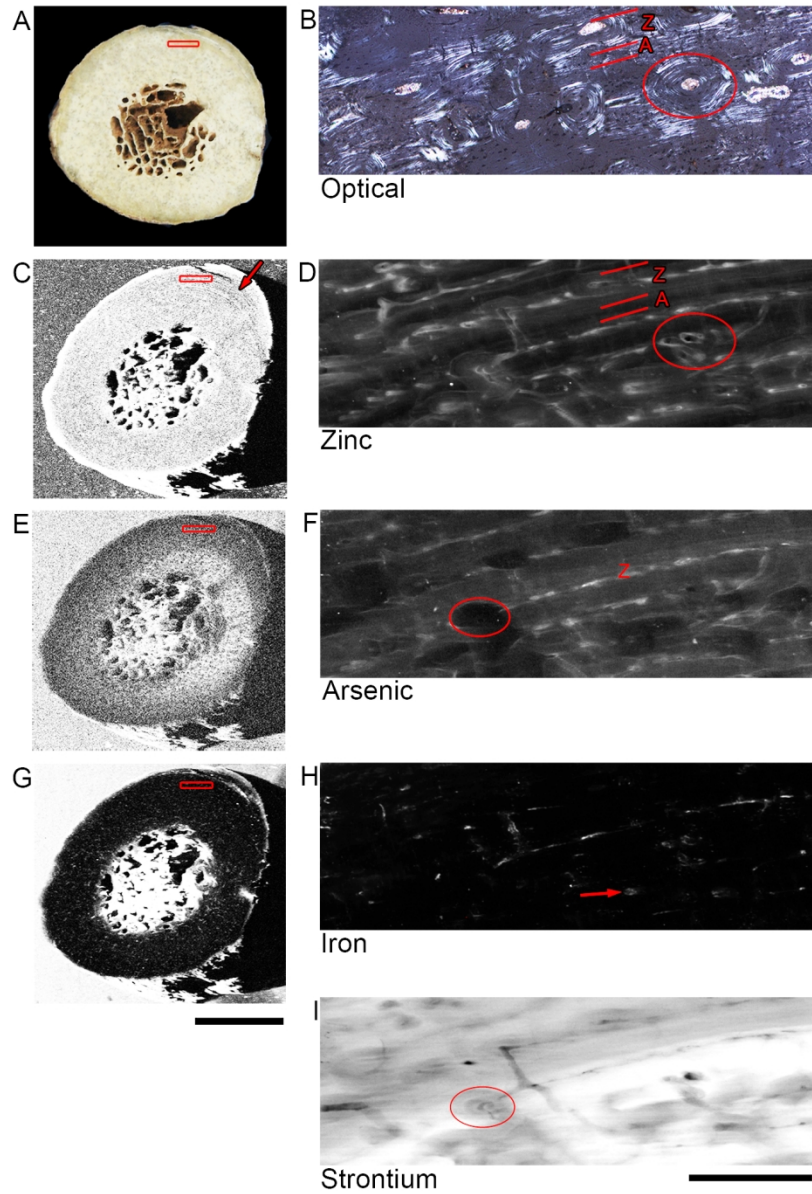


Figure 4: Fossil hyena XRF maps

117x172mm (300 x 300 DPI)

1
2
3
4
5
6
7
8
9
10
11
12
13
14
15
16
17
18
19
20
21
22
23
24
25
26
27
28
29
30
31
32
33
34
35
36
37
38
39
40
41
42
43
44
45
46
47
48
49
50
51
52
53
54
55
56
57
58
59
60

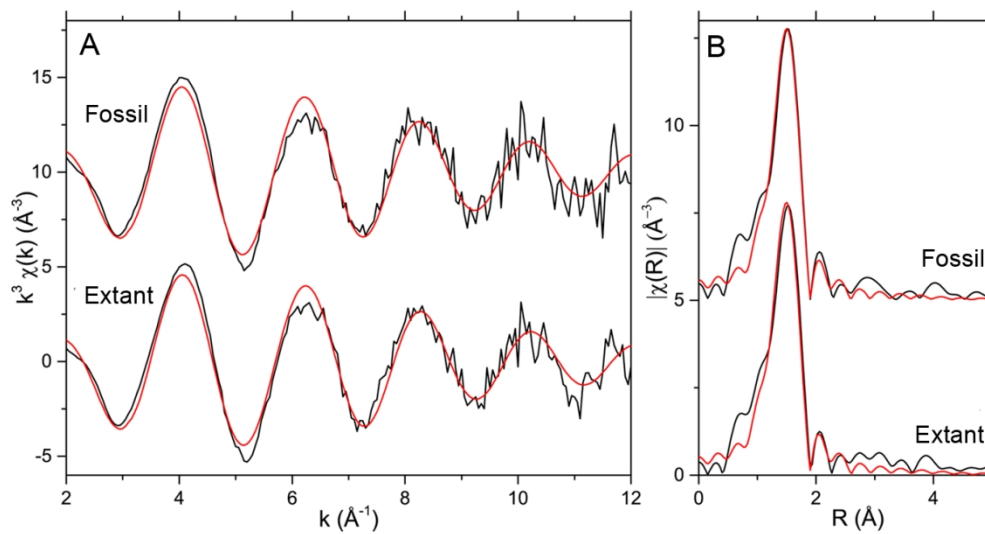


Figure 5: Zn EXAFS for extant and fossil hyena

117x61mm (300 x 300 DPI)